

• 土木工程 •

DOI:10.12454/j.jsuese.202301076



本刊网刊

基于虚拟桩法的长板-短桩多元排水体复合地基固结模型与解答

许宝龙, 卢萌盟*, 张鑫岩, 刘元杰

(中国矿业大学 力学与土木工程学院, 江苏 徐州 221116)

摘要:多元排水体复合地基能联合不同排水能力的增强体共同处理软土地基,有效加速地基固结。考虑4种工程中常见的复合地基桩-板布置形式,建立长排水板(PVD)结合短碎石桩的长板-短桩多元排水体复合地基固结解析模型,通过假设碎石桩底部存在虚拟桩,定义其固结参数与周围土体相同,保证上、下层地基孔压及渗流连续条件,基于等应变假设,充分考虑打设排水体时的涂抹效应和土体中流向碎石桩与排水板同时存在的径向双向渗流,结合分离变量法、线性方程和奇异矩阵的性质,推导瞬时荷载及多级荷载下该复合地基各孔压和平均固结度的解析解答,并通过与实测数据进行对比,验证解答的合理性。为进一步研究该复合地基固结规律及优化工法,对其固结性状进行参数敏感性分析,结果表明:本文理论解析解答与实测沉降数据较为吻合,可为相应复合地基实际工程提供依据;增大贯入度(碎石桩与复合地基长度之比)可有效提高复合地基固结速率,且对固结后期的速率影响较大;增大桩体渗透系数和压缩模量可加快地基固结前期速率,且随贯入度增大,影响效果越显著;与桩体参数对固结的影响规律不同,增加排水板数量和渗透系数也可加快地基固结速率,但对固结后期影响更显著;碎石桩涂抹系数对地基固结影响较大,而排水板由于尺寸较小,其涂抹系数对复合地基固结速率影响较弱。

关键词:固结;解析解;复合地基;碎石桩;排水板

中图分类号:TU443

文献标志码:A

文章编号:2096-3246(2025)06-0242-14

近年来,软土地基处理技术不断发展,砂井地基、散体材料桩复合地基与黏结材料桩复合地基固结理论逐渐完善,工程中也衍生出如排水桩与不排水桩组合型复合地基的新形式,取得了良好的工程效益^[1-4]。但随着工程规模增大,难度升级,以往的单一桩型复合地基和排水桩联合不排水桩组合型复合地基技术难以满足高含水率、高压缩性软土地基施工周期短,工后沉降小的要求,于是碎石桩结合塑料排水板联合处理软土地基的多元排水体复合地基技术应运而生,并在许多软土工程项目中展现出显著的优势^[5-6]。该地基处理技术结合碎石桩和排水板两种增强体的优势,能有效解决软土地基固结问题。首先,碎石桩具有应力集中效应可提高地基的承载力和稳定性,同时也有一定排水能力,可加快复合地基固结速率,减少地基沉降。其次,排水板具有优异的渗透性,能有效地排出地基中的水分,进一步增强地基处理效果^[7-8]。在多元

排水体复合地基中碎石桩与排水板的布置方式灵活多样,可根据具体工程需要进行合理设计。

实际软土地基工程中,由于软黏土层较厚,或工程条件受限,碎石桩难以贯穿,因此,组合桩一般采用长排水体联合短不排水桩的形式。整个地基的固结被分为桩体长度范围内地基的固结及桩端以下地基的固结两部分,研究表明,桩端以下土层的主固结沉降与次固结沉降往往是工后沉降过大的主要原因^[9-10],工程中应加以重视。同时,已有试验研究表明^[11-13],长板-短桩组合型复合地基可有效降低不均匀沉降和工后沉降,并能一定程度节约工程成本。因此,有必要对长板-短桩多元排水体复合地基固结进行研究。

许多学者对长板-短桩组合型复合地基固结问题开展了相关研究。叶观宝等^[14]对长板-短桩深厚软基工程进行2维有限元分析模拟,从数值角度分析其固结特性。司海燕等^[15]通过离心模拟试验,针对不同工况,研究

收稿日期:2023-12-28 修回日期:2024-04-17 网络出版日期:2024-04-25

基金项目:国家自然科学基金项目(52178373;51878657)

作者简介:许宝龙(1999—),男,硕士生。研究方向:地基固结理论;软黏土力学。E-mail:TS21030069A31@cumt.edu.cn

*通信作者:卢萌盟,教授,E-mail:lumm79@126.com

长板-短桩复合地基工法的加固机理和固结特性。邢皓枫等^[16]通过将排水板视为排水墙,忽略其厚度和井阻效应,并将桩体退化为土体,研究了长板-短桩复合地基固结简化解答。Yu等^[17]对透水桩与不透水桩组合型复合地基形式进行研究,基于轴对称固结模型与双层地基固结模型,给出了短不排水桩与长排水桩组合型复合地基的固结解析解答。卢萌盟等^[18]考虑排水板流入与流出水流的不同状态,创新性地采用环形等效的方式考虑排水板的排水能力。黄生根等^[19]依据卢萌盟等^[18]排水板环形等效法,采用修正后的流量相等假设,基于轴对称条件和等应变假设,得到了任意荷载下的长板-短桩复合地基固结解析解答。然而,目前尚无针对长排水板结合短碎石桩的长板-短桩多元排水体复合地基的固结理论解析模型与解答。

为研究此类复合地基固结问题,参考谢康和等^[20]的虚拟井法,该方法在研究未打穿砂井复合地基时,通过在下层土体中设置虚拟排水井,考虑虚拟井渗流参数与原状土保持一致,更好地考虑砂井底端的连续性条件,从而得到未打穿砂井地基复合固结解答。通过将该解答与其他解答进行对比,验证虚拟井法的可靠性。同样,可通过在碎石桩底部设置一虚拟桩的形式,考虑碎石桩在桩底深度处的孔压连续性,从而研究长板-短桩多元排水体复合地基固结理论,将该方法称为虚拟桩法。

本文针对长板-短桩多元排水体复合地基,基于轴对称固结理论与等应变假设,以碎石桩为中心,塑料排水板为边界进行单元选取,通过在碎石桩底部设置虚拟桩,完善边界条件,建立考虑碎石桩打穿部分及桩端以下部分土体内均存在流向中心碎石桩与外围排水板双向渗流的固结模型,利用傅里叶变换及线性方程组等数学物理方法,推导瞬时荷载与多级瞬时荷载下的长板-短桩多元排水体复合地基固结解析解答,进一步结合工程实例验证解答的合理性,并通过参数敏感性分析,对该复合地基固结性状进行进一步研究。

1 模型建立与基本假定

研究长板-短桩多元排水体复合地基固结问题,首先需考虑碎石桩与塑料排水板的布置形式。为使解答更具普遍性,提出 4 种多元排水体复合地基布置模式,分别为三角形、正方形、密集型三角形和密集型正方形布置,具体如图 1 所示。图 1 中, l 为碎石桩间距,空白处为土体,长方形板为排水板,圆形为碎石桩。划分单元时以碎石桩为中心,排水板为边界,将整个地基划分为一系列相同的桩-板-土单元。排水板位于单元棱角处,各排水板分配给每个单元的面积正好构成 n_w 个完整的排水板^[21-22]。不同的复合地基布置形式对应的

排水板数量 n_w 不同,三角形布置及正方形布置时,单元内排水板面积恰好为一个排水板面积, $n_w=1$; 密集型三角形布置时,单元内排水板构成的面积为两个排水板面积, $n_w=2$; 密集型正方形布置时,单元内排水板构成的面积则为 3 个排水板面积, $n_w=3$ 。以三角形桩-板布置形式为例,参考 Lu 等^[22]的单元划分法,按面积等效原则,将六边形单元等效为圆形单元,同时将排水板等效为一个面积不变且连续分布在单元外围的环形排水区,最终形成一个包含桩-土-板三元体系的固结单元,如图 2 所示。图 2 中: r_c 为模型中心碎石桩的半径,按实际取值; r_e 为土体外边界半径; r_n 为单元外径; r_{sw} 为外涂抹区范围中 n_w 个排水板扰动面积之和; r_{sc} 为内涂抹区半径与传统单个碎石桩的涂抹区半径,二者相同; r 为径向距离; h_1 为碎石桩打穿深度; h_2 为桩端以下深度; H 为复合地基总深度。对于桩-板正方形布置、密集型三角形布置和密集型正方形布置形式也可采用类似方法进行单元划分与选取,其等效形成的桩-土-板柱形单元与三角形布置时相同。

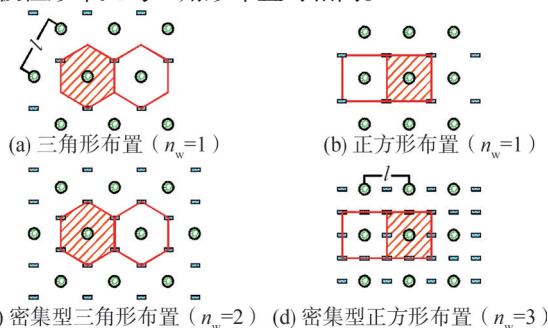


图 1 桩-板布置形式与单元划分

Fig. 1 Stone columns-PVDs layout and element partition

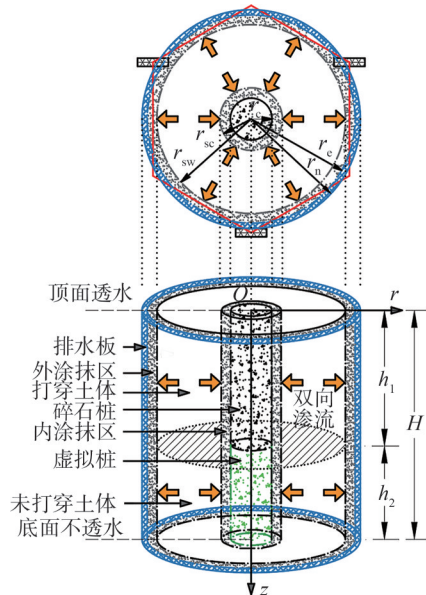


图 2 长板-短桩多元排水体复合地基固结模型

Fig. 2 Consolidation model for composite foundation with long PVDs and short stone columns

图 2 将长排水板-短碎石桩多元排水体复合地基分为两层,上层为碎石桩打穿部分地基,下层为碎石桩桩端以下部分地基。为使复合地基上、下层渗流条件相同且孔压连续,参考谢康和等^[20]的虚拟井法,将桩径范围内且位于碎石桩底部以下的土体视为虚拟桩体,即假设碎石桩底部存在一半径同样为 r_c 的虚拟碎石桩,该虚拟碎石桩的渗透系数和压缩模量与下层地基原状土相同,即可在上、下层复合地基中均考虑土体双向渗流固结,且保证碎石桩底部孔压与渗流条件的连续性。

该模型中, r_n 由桩体间距决定,可通过面积相等原则分别确定为 $r_n=0.525l$ (三角形布置)或 $r_n=0.565l$ (正方形布置)。

工程中常用的排水板为薄板矩形结构,计算时需将排水板截面积等效为单元外圆环面积,即图 2 中 $r_c \sim r_n$ 之间的环形部分。土体中孔隙水向外流入排水板后沿竖向排出, r_e 计算公式为:

$$r_e = \pi(r_n^2 - r_c^2) = n_w ab \quad (1)$$

式中, a 、 b 分别为排水板的宽度与厚度。

为便于计算,以 r_w 表示排水板的等效半径, $r_w = \sqrt{n_w ab/\pi}$ 。

打入排水板与碎石桩时会对周围土体产生扰动,该模型单元中,打设塑料排水板时产生的涂抹区称为外涂抹区,打设碎石桩时产生的涂抹区称为内涂抹区。 r_{sw} 可表示为:

$$r_{sw} = \sqrt{r_c^2 - n_w(r_{sw0}^2 - ab/\pi)} \quad (2)$$

式中, r_{sw0} 为单个排水板引起的涂抹区半径。

考虑涂抹效应的地基土体径向渗透系数 $k_{ri}(r)$,其表达式为:

$$k_{ri}(r) = k_{hi} f_i(r) \quad (3)$$

式中: k_{hi} 为第 i 层原状土的径向渗透系数, $i=1,2$; $f_i(r)$ 为土体径向渗透系数在涂抹区与非涂抹区的变化系数,其表达式为:

$$f_i(r) = \begin{cases} \frac{k_{sci}}{k_{hi}} = \alpha_{ci}, r_c < r \leq r_{sc}; \\ 1, r_{sc} < r < r_{sw}; \\ \frac{k_{swi}}{k_{hi}} = \alpha_w, r_{sw} \leq r < r_c \end{cases} \quad (4)$$

式中: k_{sci} 为内涂抹区内第 i 层地基土渗透系数; α_{ci} 为第 i 层地基土中碎石桩的扰动效应; k_{swi} 为外涂抹区内第 i 层地基土渗透系数; α_w 为地基土中排水板的扰动效应,上、下层排水板扰动效应差别不大,因此用同一符号表示。

为建立长板-短桩多元排水体复合地基固结模型,

还需作如下假设:

- 1) 土体饱和,土颗粒和水不可压缩;
- 2) 固结过程中渗透系数与压缩模量保持不变;
- 3) 孔隙水渗流服从达西定律;
- 4) 等应变条件成立,上、下层中同一深度处碎石桩、土体与排水板仅存在竖向应变,且应变相等,即上层地基中碎石桩、土体、排水板应变均为 ε_{v1} ,下层地基中土体、排水板应变均为 ε_{v2} ;
- 5) 考虑土体水仅沿径向渗流,已有研究表明,复合地基中土体径向渗流占主导地位,是否考虑竖向渗流对计算结果影响很小^[23-24],因此,忽略土体中的竖向渗流;
- 6) 上、下层塑料排水板的渗透系数和压缩系数相同;
- 7) 荷载一次瞬时施加。

2 控制方程推导及解答

2.1 定解条件

基于已有研究和以上假定,土体径向固结方程可表示为:

$$\frac{1}{r} \cdot \frac{\partial}{\partial r} \left(\frac{k_{ri}(r)}{\gamma_w} r \frac{\partial u_{si}}{\partial r} \right) = - \frac{\partial \varepsilon_{vi}}{\partial t} \quad (5)$$

式中: ε_{vi} 为第 i 层地基的竖向应变; u_{si} 为第 i 层地基土体的超孔隙水压力,其中, u_{s2} 定义为第2层地基土体内的超孔隙水压力,第2层地基土体指的是第2层中半径位于 $r_c \sim r_e$ 范围内的土体,半径位于 $0 \sim r_c$ 范围内的土体被视为虚拟桩; γ_w 为水的重度; t 为时间。

由等应变假设,可将上、下层地基竖向应变表示为:

$$\varepsilon_{vi} = \frac{\bar{\sigma} - \bar{u}_i}{E_{comi}} \quad (6)$$

式中, $\bar{\sigma}$ 为总应力, \bar{u}_i 为第 i 层地基的复合地基平均孔压, E_{comi} 为第 i 层地基的复合压缩模量。

第 i 层复合地基的压缩模量与平均孔压分别为:

$$E_{comi} = \frac{E_{ci} r_c^2 + E_{si} (r_e^2 - r_c^2) + E_w (r_n^2 - r_c^2)}{r_n^2} \quad (7)$$

$$\bar{u}_i = \frac{\bar{u}_{ci} r_c^2 + \bar{u}_{si} (r_e^2 - r_c^2) + \bar{u}_{wi} (r_n^2 - r_c^2)}{r_n^2} \quad (8)$$

式(7)、(8)中: \bar{u}_{ci} 、 \bar{u}_{wi} 、 \bar{u}_{si} 分别为第 i 层地基内的桩体平均孔压、排水板平均孔压与土体平均孔压,其中, \bar{u}_{c2} 为第2层虚拟桩内的平均孔压, \bar{u}_{s2} 为第2层地基土体的平均孔压; E_{ci} 、 E_w 、 E_{si} 为第 i 层地基桩体压缩模量、排水板压缩模量、土体压缩模量,其中, E_{c2} 为第2层地基内虚拟桩的压缩模量,与第2层地基土体压缩模量 E_{s2} 相同。

土体平均孔压 \bar{u}_{si} 表达式为:

$$\bar{u}_{si} = \frac{1}{\pi(r_c^2 - r_c'^2)} \int_{r_c'}^{r_c} 2\pi r u_{si} dr \quad (9)$$

桩-土界面处连续性条件为:

$$r = r_c : u_{si} = u_{ci} \quad (10)$$

$$r = r_c : 2\pi r \frac{k_{ri}(r)}{\gamma_w} \cdot \frac{\partial u_{si}}{\partial r} = -\pi r_c^2 \frac{k_{ci}}{\gamma_w} \cdot \frac{\partial^2 \bar{u}_{ci}}{\partial z^2} \quad (11)$$

式(10)、(11)中: u_{ci} 为第*i*层地基内桩体孔压,由于不考虑碎石桩内径向渗流,则 $u_{ci} = \bar{u}_{ci}$; k_{ci} 为第*i*层桩体渗透系数,其中, k_{c1} 为第1层碎石桩的渗透系数, k_{c2} 为第2层虚拟桩的渗透系数,与第2层地基土体渗透系数相同; z 为深度。

排水板-土界面处连续性条件为:

$$r = r_c : u_{si} = u_{wi} \quad (12)$$

$$r = r_c : 2\pi r \frac{k_{ri}(r)}{\gamma_w} \cdot \frac{\partial u_{si}}{\partial r} = \pi r_w^2 \frac{k_w}{\gamma_w} \cdot \frac{\partial^2 \bar{u}_{wi}}{\partial z^2} \quad (13)$$

式(12)、(13)中: u_{wi} 为第*i*层地基内排水板孔压,不考虑排水板内径向渗流,则 $u_{wi} = \bar{u}_{wi}$; k_w 为塑料排水板渗透系数。

通过定义上层与下层地基边界处土体孔压连续、排水板孔压连续、碎石桩与虚拟桩孔压连续、碎石桩与虚拟桩流速连续,可设定解连续条件为:

$$z = h_1 : \bar{u}_{s1} = \bar{u}_{s2} \quad (14)$$

$$z = h_1 : \bar{u}_{w1} = \bar{u}_{w2} \quad (15)$$

$$z = h_1 : \bar{u}_{c1} = \bar{u}_{c2} \quad (16)$$

$$z = h_1 : k_{c1} \frac{\partial \bar{u}_{c1}}{\partial z} = k_{c2} \frac{\partial \bar{u}_{c2}}{\partial z} \quad (17)$$

地基表面与底面排水条件为:

$$z = 0 : \bar{u}_1 = \bar{u}_c = \bar{u}_{s1} = \bar{u}_{w1} = 0 \quad (18)$$

$$z = H : \frac{\partial \bar{u}_2}{\partial z} = \frac{\partial \bar{u}_{s2}}{\partial z} = \frac{\partial \bar{u}_{w2}}{\partial z} = 0 \quad (19)$$

初始条件为:

$$t = 0 : \bar{u}_1 = \bar{u}_2 = p_0 \quad (20)$$

式中, p_0 为瞬时施加的外荷载。

2.2 控制方程

对固结方程移项、积分可得:

$$\frac{k_{ri}(r)}{\gamma_w} r \frac{\partial u_{si}}{\partial r} = - \frac{\partial \varepsilon_{vi}}{\partial t} \cdot \frac{r^2}{2} + C_i \quad (21)$$

式中, C_i 为常数。

对式(21)移项、积分,结合式(10)得:

$$u_{si} = \bar{u}_{ci} - \frac{\partial \varepsilon_{vi}}{\partial t} \cdot \frac{\gamma_w}{2k_{hi}} B_0(r) + C_i \frac{\gamma_w}{k_{hi}} A_0(r) \quad (22)$$

式中, $A_0(r) = \int_{r_c'}^r \frac{1}{x f_i(x)} dx$, $B_0(r) = \int_{r_c'}^r \frac{x}{f_i(x)} dx$, 其中, x 为

积分变量。

结合边界条件式(12)和(22),得:

$$C_i = \frac{k_{hi}}{\gamma_w} \cdot \frac{\bar{u}_{wi} - \bar{u}_{ci}}{A_0(r_c)} + \frac{B_0(r_c)}{2A_0(r_c)} \cdot \frac{\partial \varepsilon_{vi}}{\partial t} \quad (23)$$

将式(23)代回式(22)得 \bar{u}_{si} 表达式:

$$\bar{u}_{si} = \frac{\partial \varepsilon_{vi}}{\partial t} \cdot \frac{\gamma_w}{2k_{hi}} \left(\frac{B_0(r_c)}{A_0(r_c)} A_0(r) - B_0(r) \right) + \left(1 - \frac{A_0(r)}{A_0(r_c)} \right) \bar{u}_{ci} + \frac{A_0(r)}{A_0(r_c)} \bar{u}_{wi} \quad (24)$$

结合式(9)与(24)得土体平均孔压为:

$$\bar{u}_{si} = \left(\frac{\partial \varepsilon_{vi}}{\partial t} \cdot \frac{\gamma_w}{k_{hi}} \left(\frac{B_0(r_c)}{A_0(r_c)} A_1 - B_1 \right) + \left(r_c^2 - r_c'^2 - \frac{2A_1}{A_0(r_c)} \right) \bar{u}_{ci} + \frac{2A_1}{A_0(r_c)} \bar{u}_{wi} \right) / (r_c^2 - r_c'^2) \quad (25)$$

式中, $A_1 = \int_{r_c'}^{r_c} r A_0(r) dr$, $B_1 = \int_{r_c'}^{r_c} r B_0(r) dr$ 。

进一步结合式(8)与(25),可得复合地基平均孔压表达式为:

$$\bar{u}_i = \left(\frac{r_c^2}{r_n^2} - \frac{2A_1}{A_0(r_c)r_n^2} \right) \bar{u}_{ci} + \left(\frac{r_w^2}{r_n^2} + \frac{2A_1}{A_0(r_c)r_n^2} \right) \bar{u}_{wi} + \frac{B_0(r_c)A_1 - A_0(r_c)B_1}{r_n^2 A_0(r_c)} \cdot \frac{\gamma_w}{k_{hi}} \cdot \frac{\partial \varepsilon_{vi}}{\partial t} \quad (26)$$

联立边界条件式(11)、(13)与(21),得:

$$\bar{u}_{wi} = \bar{u}_{ci} - r_c^2 A_0(r_c) \frac{k_{ci}}{2k_{hi}} \cdot \frac{\partial^2 \bar{u}_{ci}}{\partial z^2} + \left(A_0(r_c)r_c^2 - B_0(r_c) \right) \frac{\gamma_w}{2k_{hi}} \cdot \frac{\partial \varepsilon_{vi}}{\partial t} \quad (27)$$

$$\frac{\partial^2 \bar{u}_{wi}}{\partial z^2} = - \frac{\partial^2 \bar{u}_{ci}}{\partial z^2} \cdot \frac{k_c}{k_w} \cdot \frac{r_c^2}{r_w^2} - \frac{\partial \varepsilon_{vi}}{\partial t} \cdot \frac{\gamma_w}{k_w} \cdot \frac{r_c^2 - r_c'^2}{r_w^2} \quad (28)$$

将式(6)对*t*求1阶偏导,联立式(26)、(27),可得:

$$\bar{u}_i = \bar{u}_{ci} - R_{i1} \frac{\partial^2 \bar{u}_{ci}}{\partial z^2} - R_{i2} \frac{\partial \bar{u}_i}{\partial t} \quad (29)$$

式中, $R_{i1} = (r_w^2 A_0(r_c) + 2A_1) \frac{r_c^2}{r_n^2} \cdot \frac{k_{ci}}{2k_{hi}}$, $R_{i2} = (r_w^2 r_c^2 A_0(r_c) - B_0(r_c) + 2r_c^2 A_1 - 2B_1) \frac{1}{r_n^2} \cdot \frac{\gamma_w}{2k_{hi} E_{comi}}$ 。

将式(26)对*z*求2阶偏导,联立式(6)、(28),可得:

$$\frac{\partial^2 \bar{u}_i}{\partial z^2} = -R_{i3} \frac{\partial^3 \bar{u}_i}{\partial t \partial z^2} + R_{i4} \frac{\partial^2 \bar{u}_{ci}}{\partial z^2} + R_{i5} \frac{\partial \bar{u}_i}{\partial t} \quad (30)$$

式中, $R_{i3} = \frac{B_0(r_c)A_1 - A_0(r_c)B_1}{r_n^2 A_0(r_c)} \cdot \frac{\gamma_w}{k_{hi} E_{comi}}$, $R_{i4} = \frac{r_c^2}{r_n^2} - \frac{r_c^2}{r_n^2} \cdot \frac{k_{ci}}{k_w} - \frac{2A_1}{A_0(r_c)r_n^2} \left(1 + \frac{r_c^2}{r_w^2} \cdot \frac{k_{ci}}{k_w} \right)$, $R_{i5} = \left(\frac{r_w^2}{r_n^2} + \frac{2A_1}{A_0(r_c)r_n^2} \right)$

$$\frac{r_c^2 - r_c^2}{r_w^2} \cdot \frac{\gamma_w}{k_w E_{com1}}$$

将式(30)代入式(29)消去 $\frac{\partial^2 \bar{u}_{ci}}{\partial z^2}$, 可得 \bar{u}_{ci} 与 \bar{u} 关系

式为:

$$\bar{u}_{ci} = \bar{u}_i + \left(R_{i2} - \frac{R_{i1} R_{i5}}{R_{i4}} \right) \frac{\partial \bar{u}_i}{\partial t} + \frac{R_{i1}}{R_{i4}} \cdot \frac{\partial^2 \bar{u}_i}{\partial z^2} + \frac{R_{i1} R_{i3}}{R_{i4}} \cdot \frac{\partial^3 \bar{u}_i}{\partial t \partial z^2} \quad (31)$$

最终, 将式(31)对 z 求 2 阶偏导与式(30)联立再次

消去 $\frac{\partial^2 \bar{u}_{ci}}{\partial z^2}$, 即得土体固结控制偏微分方程为:

$$Q_i \frac{\partial^5 \bar{u}_i}{\partial t \partial z^4} + W_i \frac{\partial^4 \bar{u}_i}{\partial z^4} + S_i \frac{\partial^3 \bar{u}_i}{\partial t \partial z^2} + D_i \frac{\partial^2 \bar{u}_i}{\partial z^2} + F_i \frac{\partial \bar{u}_i}{\partial t} = 0 \quad (32)$$

式中, $Q_i = R_{i1} R_{i3}$, $W_i = R_{i1}$, $S_i = R_{i2} R_{i4} - R_{i1} R_{i5} - R_{i3}$, $D_i = R_{i4} - 1$, $F_i = R_{i5}$ 。

2.3 方程求解

2.3.1 单级瞬时荷载下的解答

采用分离变量法对固结偏微分方程式(32)进行求解, 按 Lu 等^[25]对此类问题的解法, 设孔压为:

$$\bar{u}_i = \sum_{m=1}^{\infty} T_m(t) Z_{mi}(z) \quad (33)$$

式中, $T_m(t)$ 为与 t 相关的函数, $Z_{mi}(z)$ 为与 z 相关的函数, $m=1, 2, \dots, \infty$ 。

将孔压表达式(33)代回固结微分控制方程式(32), 经分离变量后, 可得恒等式:

$$-\frac{W_i \frac{d^4}{dz^4} Z_{mi}(z) + D_i \frac{d^2}{dz^2} Z_{mi}^{(4)}(z)}{Q_i \frac{d^4}{dz^4} Z_{mi}(z) + S_i \frac{d^2}{dz^2} Z_{mi}(z) + F_i} = \frac{d}{dt} \frac{T_m(t)}{T_m(t)} = -\beta_m \quad (34)$$

式中, β 为常数。

通过求解微分方程, 得 $T_m(t)$ 表达式为:

$$T_m(t) = A_m e^{-\beta_m t} \quad (35)$$

式中, A_m 为任意常数。

利用数学物理方法, 可求得 $Z_{mi}(z)$ 表达式为:

$$Z_{mi}(z) = a_{mi} \sin(\lambda_{mi} z) + b_{mi} \cos(\lambda_{mi} z) + c_{mi} \sinh(\xi_{mi} z) + d_{mi} \cosh(\xi_{mi} z) \quad (36)$$

式中: a_{mi} 、 b_{mi} 、 c_{mi} 、 d_{mi} 为任意常数, 由初始条件决定;

$$\lambda_{mi} = \sqrt{\frac{(D_i - S_i \beta_m) + \sqrt{(D_i - S_i \beta_m)^2 + 4(W_i - Q_i \beta_m) F_i \beta_m}}{2(W_i - Q_i \beta_m)}};$$

$$\xi_{mi} = \sqrt{\frac{-(D_i - S_i \beta_m) + \sqrt{(D_i - S_i \beta_m)^2 + 4(W_i - Q_i \beta_m) F_i \beta_m}}{2(W_i - Q_i \beta_m)}}。$$

结合式(8)、(27)、(31)及竖向边界条件式(18)和

(19), 整合式子, 可得:

$$\bar{u}_i = \sum_{m=1}^{\infty} A_m e^{-\beta_m t} Z_{mi}(z) \quad (37)$$

$$\bar{u}_{ci} = \sum_{m=1}^{\infty} A_m e^{-\beta_m t} Z_{cmi}(z) \quad (38)$$

$$\bar{u}_{wi} = \sum_{m=1}^{\infty} A_m e^{-\beta_m t} Z_{wmi}(z) \quad (39)$$

$$\bar{u}_{si} = \sum_{m=1}^{\infty} A_m e^{-\beta_m t} Z_{smi}(z) \quad (40)$$

式(38)~(40)中, $Z_{cmi}(z)$ 、 $Z_{wmi}(z)$ 、 $Z_{smi}(z)$ 为碎石桩、排水板、土体平均孔压表达式中与深度 z 相关的函数。

$$\begin{cases} Z_{m1}(z) = a_{m1} \sin(\lambda_{m1} z) + c_{m1} \sinh(\xi_{m1} z), \\ Z_{m2}(z) = b_{m2} \cos(\lambda_{m2}(H-z)) + d_{m2} \cosh(\xi_{m2}(H-z)) \end{cases} \quad (41)$$

$$\begin{cases} Z_{cm1}(z) = a_{m1} K_a \sin(\lambda_{m1} z) + c_{m1} K_c \sinh(\xi_{m1} z), \\ Z_{cm2}(z) = b_{m2} K_b \cos(\lambda_{m2}(H-z)) + d_{m2} K_d \cosh(\xi_{m2}(H-z)) \end{cases} \quad (42)$$

$$\begin{cases} Z_{wmi}(z) = a_{m1} L_a \sin(\lambda_{m1} z) + c_{m1} L_c \sinh(\xi_{m1} z), \\ Z_{wm2}(z) = b_{m2} L_b \cos(\lambda_{m2}(H-z)) + d_{m2} L_d \cosh(\xi_{m2}(H-z)) \end{cases} \quad (43)$$

$$\begin{cases} Z_{sm1}(z) = a_{m1} \psi_a \sin(\lambda_{m1} z) + c_{m1} \psi_c \sinh(\xi_{m1} z), \\ Z_{sm2}(z) = b_{m2} \psi_b \cos(\lambda_{m2}(H-z)) + d_{m2} \psi_d \cosh(\xi_{m2}(H-z)) \end{cases} \quad (44)$$

式(42)~(44)中,

$$K_a = 1 - \frac{S_1 + \frac{Q_1}{W_1}}{D_1 + 1} \beta_m - \frac{W_1}{D_1 + 1} \lambda_{m1}^2 + \frac{Q_1}{D_1 + 1} \lambda_{m1}^2 \beta_m,$$

$$K_b = 1 - \frac{S_2 + \frac{Q_2}{W_2}}{D_2 + 1} \beta_m - \frac{W_2}{D_2 + 1} \lambda_{m2}^2 + \frac{Q_2}{D_2 + 1} \lambda_{m2}^2 \beta_m,$$

$$K_c = 1 - \frac{S_1 + \frac{Q_1}{W_1}}{D_1 + 1} \beta_m + \frac{W_1}{D_1 + 1} \xi_{m1}^2 - \frac{Q_1}{D_1 + 1} \xi_{m1}^2 \beta_m,$$

$$K_d = 1 - \frac{S_2 + \frac{Q_2}{W_2}}{D_2 + 1} \beta_m + \frac{W_2}{D_2 + 1} \xi_{m2}^2 - \frac{Q_2}{D_2 + 1} \xi_{m2}^2 \beta_m, \quad L_a =$$

$$\left(1 + r_c^2 A_0(r_c) \frac{k_{c1}}{2k_{h1}} \lambda_{m1}^2 \right) K_a + \left(A_0(r_c) r_c^2 - B_0(r_c) \right) \frac{\gamma_w}{2k_{h1} E_{com1}} \beta_m,$$

$$L_b = \left(1 + r_c^2 A_0(r_c) \frac{k_{c2}}{2k_{h2}} \lambda_{m2}^2 \right) K_b + \left(A_0(r_c) r_c^2 - B_0(r_c) \right)$$

$$\frac{\gamma_w}{2k_{h2} E_{com2}} \beta_m, \quad L_c = \left(1 - r_c^2 A_0(r_c) \frac{k_{c1}}{2k_{h1}} \xi_{m1}^2 \right) K_c + \left(A_0(r_c) r_c^2 -$$

$$B_0(r_c) \right) \frac{\gamma_w}{2k_{h1} E_{com1}} \beta_m, \quad L_d = \left(1 - r_c^2 A_0(r_c) \frac{k_{c2}}{2k_{h2}} \xi_{m2}^2 \right) K_d +$$

$$\begin{aligned} & (A_0(r_c)r_c^2 - B_0(r_c)) \frac{\gamma_w}{2k_{h2}E_{com2}} \beta_m, \psi_a = \frac{r_n^2}{r_c^2 - r_c^2} - \frac{r_c^2}{r_c^2 - r_c^2} K_a - \\ & \frac{r_w^2}{r_c^2 - r_c^2} L_a, \psi_b = \frac{r_n^2}{r_c^2 - r_c^2} - \frac{r_c^2}{r_c^2 - r_c^2} K_b - \frac{r_w^2}{r_c^2 - r_c^2} L_b, \psi_c = \\ & \frac{r_n^2}{r_c^2 - r_c^2} - \frac{r_c^2}{r_c^2 - r_c^2} K_c - \frac{r_w^2}{r_c^2 - r_c^2} L_c, \psi_d = \frac{r_n^2}{r_c^2 - r_c^2} - \frac{r_c^2}{r_c^2 - r_c^2} K_d - \\ & \frac{r_w^2}{r_c^2 - r_c^2} L_d \end{aligned}$$

为求得 $\beta_m, a_{m1}, b_{m2}, c_{m1}, d_{m2}$, 结合边界条件式(14)~(17), 可得到线性方程为:

$$EX^T = 0 \tag{45}$$

$$X = [a_{m1} \ b_{m2} \ c_{m1} \ d_{m2}] \tag{46}$$

$$E = \begin{bmatrix} E_{11} & E_{12} & E_{13} & E_{14} \\ E_{21} & E_{22} & E_{23} & E_{24} \\ E_{31} & E_{32} & E_{33} & E_{34} \\ E_{41} & E_{42} & E_{43} & E_{44} \end{bmatrix} \tag{47}$$

$$\left\{ \begin{aligned} E_{11} &= K_a \sin(\lambda_{m1} h_1), \\ E_{12} &= -K_b \cos(\lambda_{m2} h_2), \\ E_{13} &= K_c \sinh(\xi_{m1} h_1), \\ E_{14} &= -K_d \cosh(\xi_{m2} h_2), \\ E_{21} &= k_{c1} \lambda_{m1} K_a \cos(\lambda_{m1} h_1), \\ E_{22} &= -k_{c2} \lambda_{m2} K_b \sin(\lambda_{m2} h_2), \\ E_{23} &= k_{c1} \xi_{m1} K_c \cosh(\xi_{m1} h_1), \\ E_{24} &= k_{c2} \xi_{m2} K_d \sinh(\xi_{m2} h_2), \\ E_{31} &= L_a \sin(\lambda_{m1} h_1), \\ E_{32} &= -L_b \cos(\lambda_{m2} h_2), \\ E_{33} &= L_c \sinh(\xi_{m1} h_1), \\ E_{34} &= -L_d \cosh(\xi_{m2} h_2), \\ E_{41} &= \psi_a \sin(\lambda_{m1} h_1), \\ E_{42} &= -\psi_b \cos(\lambda_{m2} h_2), \\ E_{43} &= \psi_c \sinh(\xi_{m1} h_1), \\ E_{44} &= -\psi_d \cosh(\xi_{m2} h_2) \end{aligned} \right. \tag{48}$$

为使方程式(45)有非零解, 则系数矩阵 E 的行列式 $|E|$ 必须等于 0, 即可解出 $\beta_m (m = 1, 2, \dots, \infty)$ 的表达式。同时, 由于行列式 $|E|$ 必须等于 0, 系数矩阵为奇异矩阵, 此时矩阵无法满秩。将解出的 β_m 带回式(45)中无法同时解得 $a_{m1}, b_{m2}, c_{m1}, d_{m2}$ 。此处借鉴 Tang 等^[26]的研究方法, 令 $a_{m1} = 1$, 将每个 β_m 代入式(45), 即可得到其他 3 个常数, 将以上常数代入式(37)~(44), 即可得到 $\bar{u}_i, \bar{u}_{ci}, \bar{u}_{wi}, \bar{u}_{si}$ 的表达式。

至此, 解答中还有 A_m 尚未确定, 可通过复合地基孔压的三角函数正交性^[27]求解:

$$\left(\frac{1}{E_{com1}} \int_0^{h_1} Z_{m1}(z) \cdot Z_{j1}(z) dz + \frac{1}{E_{com2}} \int_{h_1}^H Z_{m2}(z) \cdot Z_{j2}(z) dz \right) = 0, m \neq j \tag{49}$$

式中, $Z_{m1}(z), Z_{m2}(z), Z_{j1}(z), Z_{j2}(z)$ 为与 z 相关的函数, 其中, 1、2 表示第 1 层或者第 2 层地基, j 为自然数。

结合初始条件式(20), 可得:

$$A_m = p_0 g_m \tag{50}$$

$$g_m = \frac{\frac{1}{E_{com1}} G_{m1} + \frac{1}{E_{com2}} G_{m2}}{\frac{1}{E_{com1}} G_{m3} + \frac{1}{E_{com2}} G_{m4}} \tag{51}$$

式(50)、(51)中, g_m 为与 m 相关的常数, $G_{m1} = \frac{a_{m1}}{\lambda_{m1}} (1 - \cos(\lambda_{m1} h_1)) + \frac{c_{m1}}{\xi_{m1}} (\cosh(\xi_{m1} h_1) - 1)$, $G_{m2} = \frac{b_{m2}}{\lambda_{m2}} \sin(\lambda_{m2} h_2) + \frac{d_{m2}}{\xi_{m2}} \sinh(\xi_{m2} h_2)$, $G_{m3} = a_{m1}^2 \left(\frac{h_1}{2} - \frac{\sin(2\lambda_{m1} h_1)}{4\lambda_{m1}} \right) + c_{m1}^2 \left(\frac{\sinh(2\xi_{m1} h_1)}{4\xi_{m1}} - \frac{h_1}{2} \right) + \frac{2a_{m1}c_{m1}}{\lambda_{m1}^2 + \xi_{m1}^2} (\xi_{m1} \sin(\lambda_{m1} h_1) \cosh(\xi_{m1} h_1) - \lambda_{m1} \sinh(\xi_{m1} h_1) \cos(\lambda_{m1} h_1))$, $G_{m4} = b_{m2}^2 \left(\frac{h_2}{2} + \frac{\sin(2\lambda_{m2} h_2)}{4\lambda_{m2}} \right) + d_{m2}^2 \left(\frac{\sinh(2\xi_{m2} h_2)}{4\xi_{m2}} + \frac{h_2}{2} \right) + \frac{2b_{m2}d_{m2}}{\lambda_{m2}^2 + \xi_{m2}^2} (\lambda_{m2} \sin(\lambda_{m2} h_2) \cosh(\xi_{m2} h_2) + \xi_{m2} \cos(\lambda_{m2} h_2) \sinh(\xi_{m2} h_2))$ 。

至此, 瞬时荷载下孔压表达式(37)~(40)各参数均已求出, 按应力定义的上、下层与复合地基总固结度 \bar{U}_1, \bar{U}_2 分别为:

$$\bar{U}_1 = \frac{\int_0^{h_1} (p_0 - \bar{u}_1) dz}{\int_0^{h_1} p_0 dz} = 1 - \frac{1}{h_1} \sum_{m=1}^{\infty} g_m e^{-\beta_m t} G_{m1} \tag{52}$$

$$\bar{U}_2 = \frac{\int_{h_1}^H (p_0 - \bar{u}_2) dz}{\int_{h_1}^H p_0 dz} = 1 - \frac{1}{h_2} \sum_{m=1}^{\infty} g_m e^{-\beta_m t} G_{m2} \tag{53}$$

$$U_p = \frac{\int_0^{h_1} (p_0 - u_1(z, t)) dz + \int_{h_1}^H (p_0 - u_2(z, t)) dz}{\int_0^H p_0 dz} = 1 - \frac{1}{H} \sum_{m=1}^{\infty} g_m e^{-\beta_m t} (G_{m1} + G_{m2}) \tag{54}$$

式中, U_p 为应力的复合地基总固结度。

2.3.2 多级瞬时荷载下的解答

基于瞬时荷载下的孔压与固结度解答, 通过叠加方式可得到多级瞬时施加荷载下的多元排水体复

合地基孔压与平均固结度解答,多级瞬时施加荷载如图 3 所示。图 3 中, p_u 为最终荷载值, t_u 为最终荷载值施加结束时间。

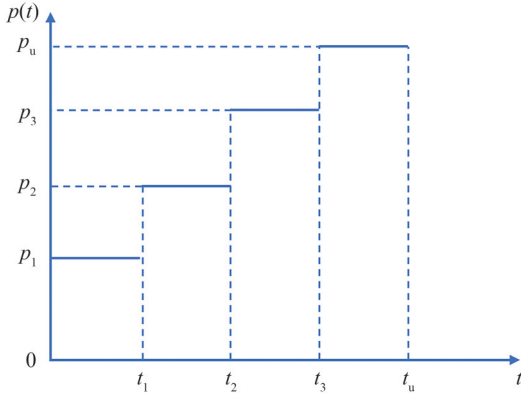


图 3 多级瞬时施加荷载

Fig.3 Multi-stage instantaneous loading

在该荷载条件下,每一级荷载施加均为连续加载过程,只是每一级荷载施加时间点不同,将任意时刻之前每一级荷载引起的孔压和平均固结度叠加,即为当前时刻多级瞬时荷载下的解答。经叠加后, k 级荷载的多元排水体复合地基固结解答可表示为:

$$\bar{u}_i = \sum_{m=1}^{\infty} g_m \left(\sum_{j=1}^k (p_j - p_{j-1}) e^{-\beta_m(t-t_{j-1})} \right) Z_{mi}(z) \quad (55)$$

式中, k 为荷载级数。

$$\bar{u}_{ci} = \sum_{m=1}^{\infty} g_m \left(\sum_{j=1}^k (p_j - p_{j-1}) e^{-\beta_m(t-t_{j-1})} \right) Z_{cmi}(z) \quad (56)$$

$$\bar{u}_{wi} = \sum_{m=1}^{\infty} g_m \left(\sum_{j=1}^k (p_j - p_{j-1}) e^{-\beta_m(t-t_{j-1})} \right) Z_{wmi}(z) \quad (57)$$

$$\bar{u}_{si} = \sum_{m=1}^{\infty} g_m \left(\sum_{j=1}^k (p_j - p_{j-1}) e^{-\beta_m(t-t_{j-1})} \right) Z_{smi}(z) \quad (58)$$

多级荷载下多元排水体复合地基平均固结度定义为土体任意时刻的有效应力与土体最终总应力之比,因此有:

$$\bar{U}_1 = \frac{\int_0^{h_1} (p_k - \bar{u}_1) dz}{\int_0^{h_1} p_u dz} = \frac{p_k}{p_u} - \frac{1}{h_1} \sum_{m=1}^{\infty} g_m \left(\sum_{j=1}^k \frac{p_j - p_{j-1}}{p_u} e^{-\beta_m(t-t_{j-1})} \right) G_{m1} \quad (59)$$

$$\bar{U}_2 = \frac{\int_{h_1}^H (p_k - \bar{u}_2) dz}{\int_{h_1}^H p_u dz} = \frac{p_k}{p_u} - \frac{1}{h_2} \sum_{m=1}^{\infty} g_m \left(\sum_{j=1}^k \frac{p_j - p_{j-1}}{p_u} e^{-\beta_m(t-t_{j-1})} \right) G_{m2} \quad (60)$$

$$U = \frac{\int_0^{h_1} (p_k - u_1(z, t)) dz + \int_{h_1}^{h_2} (p_k - u_2(z, t)) dz}{\int_0^H p_u dz} = \frac{\frac{p_k}{p_u} - \sum_{m=1}^{\infty} g_m \left(\sum_{j=1}^k \frac{p_j - p_{j-1}}{p_u} e^{-\beta_m(t-t_{j-1})} \right) (G_{m1} + G_{m2})}{H} \quad (61)$$

式(59)~(61)中, U 为平均固结度(复合地基固结度), p_k 为第 k 级荷载值。

2.4 案例验证

对解析解答进行工程实测数据对比是验证解答合理性的有效方法,可直观反映理论解答与实际工程的吻合度。Ye^[28]、Zhang^[29]等在中国上海北郊的某路堤段工程段进行了塑料排水板联合深层搅拌桩加固软土地基的承载性能试验,试验段由饱和软黏土层组成,承载能力较低。工程分为两级线性加载:首先,历时 35 d 匀速堆载至 0.7 m 高度,保持 22 d;而后历时 64 d 堆载至 3.0 m 高度,此后保持不变,填土重度为 20 kN/m³。本文将两段匀速堆载阶段视为为瞬时堆载阶段,瞬时堆载大小取匀速堆载阶段初值与终值的中间值,从而将整个加载阶段分为 4 级瞬时荷载。分级加载历时如图 4 所示。塑料排水板与深层搅拌桩采用三角形交叉布置,则 n_w 取 1,间距均为 2.5 m,其中,塑料排水板长度为 25.0 m,深层搅拌桩长度为 9.0 m。排水板规格为 100 mm×4 mm,深层搅拌桩的直径为 700 mm。由于所取工程案例中深层搅拌桩渗透性低,因此,将参数 k_{c1} 取为无穷小,即设置桩体不排水。考虑打设深层搅拌桩对周围土体的扰动较塑料排水板更大,土体涂抹区参数取 $\alpha_{c1}=0.2$, $\alpha_{c2}=1.0$, $\alpha_{w1}=\alpha_{w2}=0.3$,径向渗透系数及压缩模量采用分层加权法计算,固结参数均取自文献[28-29],如表 1 所示。

实测工程地基固结值与本文所得长板-短桩多元排水体复合地基固结解答对比如图 5 所示。二者沉降曲线在荷载过渡阶段皆有波动,且由于本文将线性堆载简化为多级瞬时堆载,因此波动较为显著,这是因为荷载的施加会使得土体孔压骤然增大,排水速率提高,加快地基固结。此外,在线性堆载阶段由于取中间值等效为瞬时荷载,因此在两端简化加载阶段理论解的固结度会先高于实测值,后低于实测值。而曲线后期理论值小于实测值的原因在于深层搅拌桩并不是完全不排水,本文解答将其设置为不排水,使得固结度偏低。对比二者曲线可知:本文解答与工程实测沉降值的整体变化趋势相同;在整个固结阶段,平均固结度曲线间差异均小于 5%,理论解答固结度与实测固

表 1 固结参数
Tab.1 Parameters of consolidation

参数	h_1/m	h_2/m	H/m	r_n/m	r_c/m	r_w/m	$k_{s1}/(m \cdot s^{-1})$	$k_{s2}/(m \cdot s^{-1})$	$k_{c1} \cdot k_{s1}^{-1}$	$k_{c2} \cdot k_{s2}^{-1}$	E_s/MPa	E_{c1}/MPa
取值	9	16	25	1.525	0.35	0.011	1.50×10^{-8}	8.83×10^{-9}	1 000	0.5	2.94	30

结度吻合度较高。表明本文解析解答可较为准确地计算长排水板-短碎石桩处理下的软土地基固结度,验证了本文解答具有较高的合理性与可靠性,可为实际工程提供依据。

$3r_w; k_{h1} = 1.6 \times 10^{-9} m/s, k_{h2} = 1.2 \times 10^{-9} m/s, k_{c1}/k_{h1} = 10^3, k_{c2}/k_{h2} = 0.5, k_w/k_{h1} = 10^4; E_{s1} = 1 MPa, E_{c1}:E_{c2}:E_w:E_{s1}:E_{s2} = 5:1:1:1:1; \alpha_{c1} = 0.2, \alpha_{c2} = 1, \alpha_{w1} = \alpha_{w2} = 0.3。$

3.1 与其他解答对比

为研究本文解答与其他形式复合地基固结解答的差异,结合碎石桩与排水板等长条件下的多元排水体复合地基固结解答^[30]与长排水板-短水泥土桩复合地基固结解答^[31],基于以上复合地基固结计算参数,分别进行求解得到固结度曲线,如图 6 所示。对碎石桩与排水板等长条件下的多元排水体复合地基固结解答,考虑两种情况:一是计算深度 $H=10 m$ (仅考虑上层碎石桩深度内复合地基的固结,忽略碎石桩端以下部分地基固结);二是计算深度 $H=15 m$ (将长板-短桩多元排水体复合地基整体视为碎石桩与排水板等长的多元排水体复合地基)。由图 6 可知,以上两种计算方式均会高估长排水板-短碎石桩条件下的多元排水体复合地基固结速率,若忽略桩端以下复合地基固结,则最大平均固结度误差可达 26%,计算结果偏于不安全。同时,情况二与本文解答固结前期曲线差异较小,而随着固结发展,固结曲线差异呈逐渐增大趋势,最大差异可达 15.9%,因此本文长板-短桩多元排水体复合地基固结解析解答对工程实践具有重要意义。此外,本文所得长排水板-短碎石桩复合地基由于碎石桩具有更大的渗透系数,固结速率明显优于长排水板-短水泥土桩复合地基。

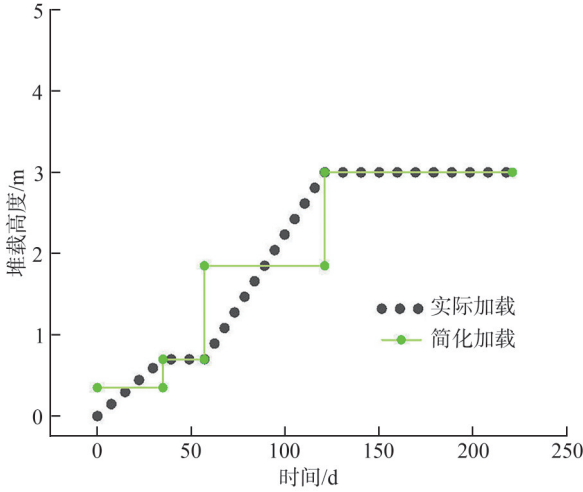


图 4 分级加载历时
Fig. 4 Duration of graded loading

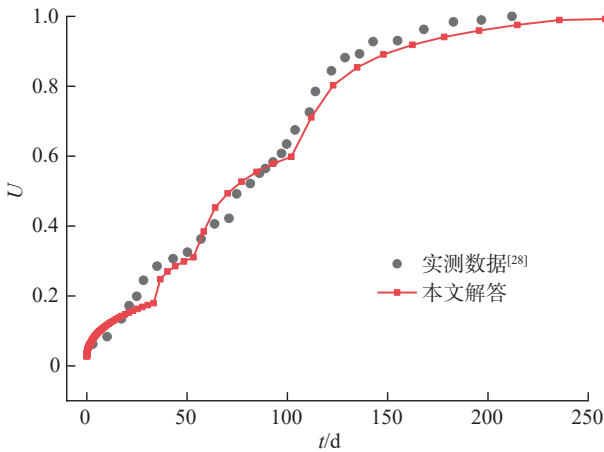


图 5 工程实测与理论结果对比
Fig. 5 Comparison of engineering measurement and theoretical results

3 固结性状分析

进一步研究长板-短桩多元排水体复合地基的固结特性,为使结果更具普遍性,统一采用无量纲固结时间因子 $T_{h1} = k_{h1} E_{s1} t / (4r_n^2 \gamma_w)$ 作为横坐标变量, U 作为纵坐标绘制固结曲线图。除单独研究变量外,固结性状分析计算参数设为: $H=15 m, h_1=10 m, h_2=5 m; L=2 m, r_c=0.3 m, a \times b=0.1 m \times 0.005 m, r_{sc}=2r_c, r_{sw0}=$

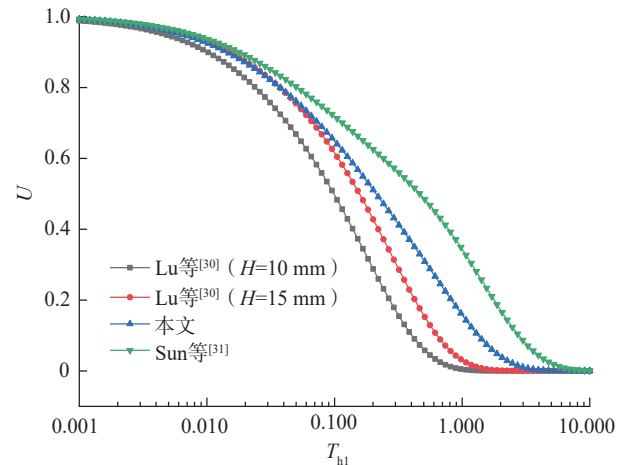


图 6 不同复合地基固结解答对比
Fig. 6 Comparison of consolidation solutions of different composite foundations

3.2 贯入度的影响

贯入度为碎石桩长度 h_1 与复合地基深度 H 之比 ($\psi=h_1/H$)。贯入度对复合地基固结度的影响如图 7 所示。由图 7 可知,贯入度越高,复合地基整体固结度越大。进一步对比不同贯入度下固结曲线可知,提高贯入度对复合地基固结后期速率的影响更大,对固结前期几乎无影响。低贯入度意味着深度方向上长板-短桩多元排水体复合地基中碎石桩端以下部分地基占比更多,而由于假设 PTIB 排水条件,深度越大,固结越慢;且上层复合地基的碎石桩具有良好的排水能力与应力集中效应,其排水固结能力较下层复合地基更强,使得前期上层地基固结在整体固结中占主导地位。因此,当上层固结条件相同时,不同贯入度条件下的前期固结速率几乎无差,固结差异主要体现在固结后期阶段。即当贯入度增大,碎石桩长度占复合地基深度的比重越大,可显著提高复合地基后期的固结速率,加快复合地基固结沉降。

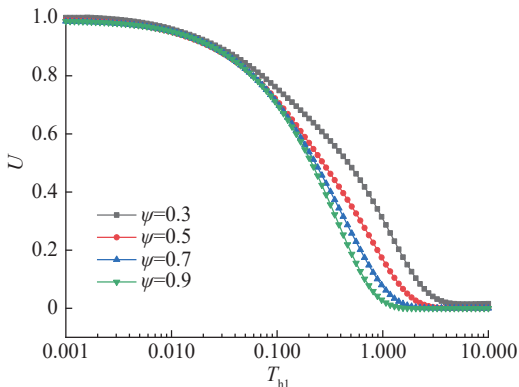


图 7 贯入度对复合地基固结度的影响

Fig. 7 Influence of penetration on the consolidation degree of composite foundation

3.3 涂抹效应的影响

图 8 为碎石桩涂抹效应 α_{c1} 与排水板涂抹效应 α_w 对复合地基固结的影响。由于下层土中采用虚拟桩,实际并未对周围土体产生扰动,因此,不考虑下层土中桩体的涂抹作用,即 $\alpha_{c2}=1$;而对外围排水板,在上、下土层引起的涂抹作用假定为相同,统一以 α_w 表示。由图 8(a)可知,随 α_{c1} 减小,复合地基固结速率变慢。对比 α_{c1} 取不同值时的固结曲线, α_{c1} 越小,曲线间的差异越大,即随扰动程度增大,对复合地基固结度的影响程度也越大。图 8(b)给出的复合地基固结速率随着 α_w 减小同样呈减慢趋势,但复合地基固结度差异不大,其原因在于排水板规格较小,相应的涂抹区范围也较小。综上可知,涂抹效应对长排水板-短碎石桩多元排水板复合地基固结有一定影响,若忽视涂抹效应会使计算结果偏于不安全。

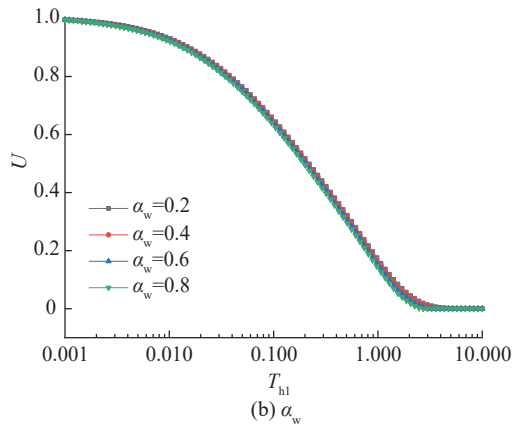
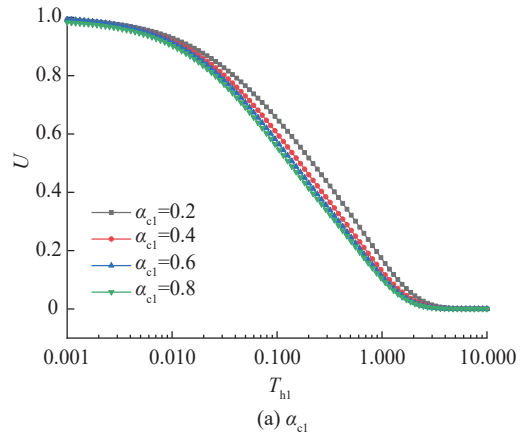


图 8 土体涂抹渗透系数对复合地基固结度的影响

Fig. 8 Influence of soil smear permeability coefficient on the consolidation degree of composite foundation

3.4 单元排水板数量的影响

图 9 为外围排水板数量 n_w 对长板-短桩多元排水体复合地基固结度的影响。由图 9 可知,随着外围排水板数量增多,复合地基整体固结速率加快,原因在于增加排水板数量可以增大外围排水体的面积,从而加快孔隙水压力的排出,加速固结。此外,由于下层地基固结较晚,且该层孔隙水主要通过排水板流出,因此增加排水板数量对固结后期速率提升更为显著。

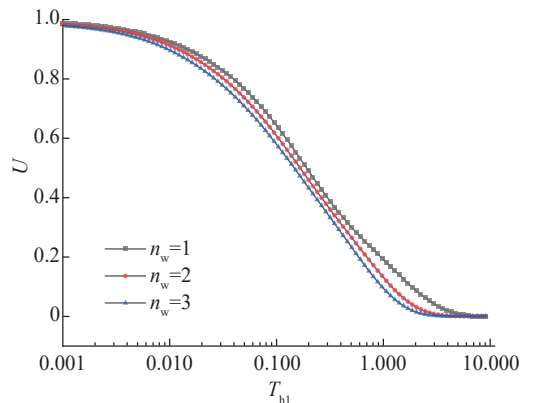


图 9 外围排水板数量对复合地基固结度的影响

Fig. 9 Influence of the number of PVDs on the consolidation degree of composite foundation

3.5 桩体与排水板渗透系数的影响

图 10、11 分别为不同贯入度 ψ 条件下碎石桩体与塑料排水板的渗透系数对长板-短桩多元排水体复合地基固结的影响。由图 10、11 可知,在不同贯入度条件下,复合地基固结速率随桩体渗透系数 k_{c1} 和排水板渗透系数 k_w 增大均有所加快。但在不同贯入度条件下, k_{c1} 与 k_w 对复合地基固结过程的影响有所差异。当 $\psi=0.9$ 时,随 k_{c1} 增大,复合地基整体固结全周期的速率均有所提高;当 $\psi=0.5$ 时,复合地基速率随 k_{c1} 增大时在固结后期增幅较前中期更小。对比图 11(a) 与 (b) 可知:当 $\psi=0.9$ 时,复合地基固结全周期速率随 k_w 增大均有明显提高;当 $\psi=0.5$ 时,不同曲线间的差异表明提高 k_w 对固结后期加速效果更为显著。即提高 k_{c1} 和 k_w 均能加快长板-短桩多元排水体复合地基固结速率,但在低贯入条件下, k_{c1} 对复合地基后期固结影响较小,而 k_w 对复合地基后期固结影响较大。

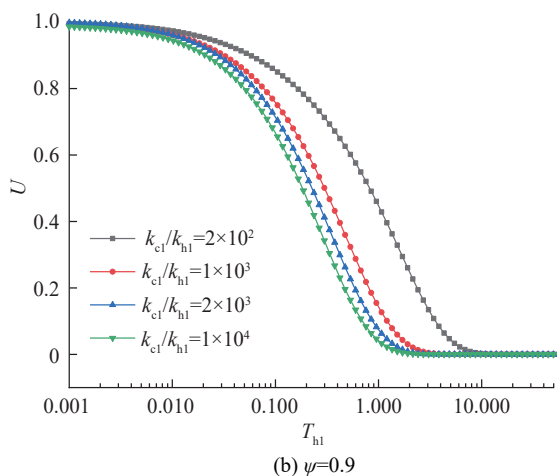
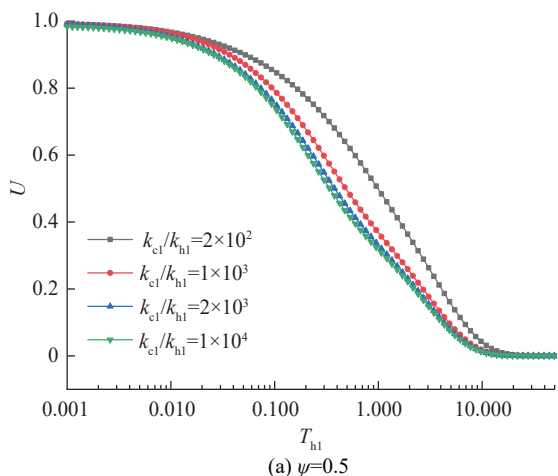


图 10 桩体渗透系数对复合地基固结度的影响
 Fig. 10 Influence of permeability coefficient of stone columns on consolidation degree of composite foundation

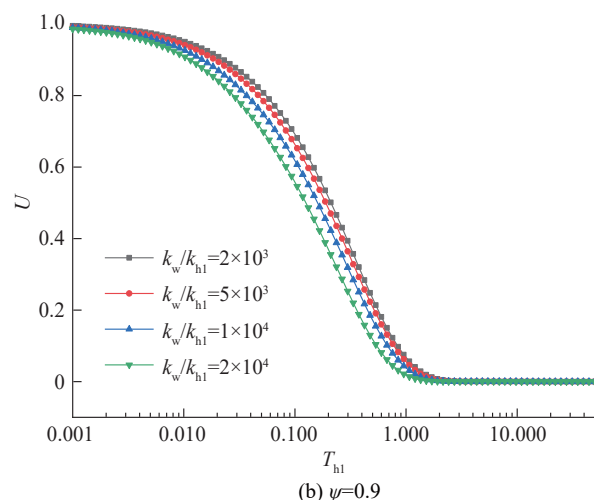
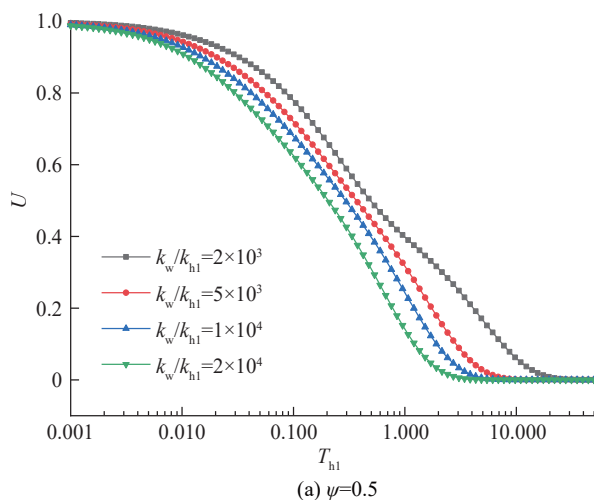


图 11 排水板渗透系数对复合地基固结度的影响
 Fig. 11 Influence of permeability coefficient of PVDs on consolidation degree of composite foundation

3.6 桩体压缩模量的影响

对不同贯入度 ψ 下,桩体压缩模量对长板-短桩多元排水体复合地基固结度的影响进行分析,如图 12 所示。由图 12 可知,随着碎石桩压缩模量 E_{c1} 增大,同一时间复合地基固结度更高,固结速率更快;更高的桩体压缩模量可使得碎石桩在复合地基中承受更大的荷载,表现出明显的应力集中现象,减小复合地基变形,从而加快固结速率。由图 12(a) 可知,随桩体压缩模量 E_{c1} 增大,低贯入度条件下的复合地基固结速率在前中期的增幅较为显著,而在固结后期几乎无变化。压缩模量 E_{c1} 仅会增大碎石桩打设范围内土体的复合压缩模量,降低上层土的变形;而固结后期主要为下层复合地基进行固结,下层桩体为虚拟桩体,其压缩模量恒等于土体压缩模量 E_s ,因此,贯入度越低, E_{c1} 对复合地基后期固结的提升效果越微弱。

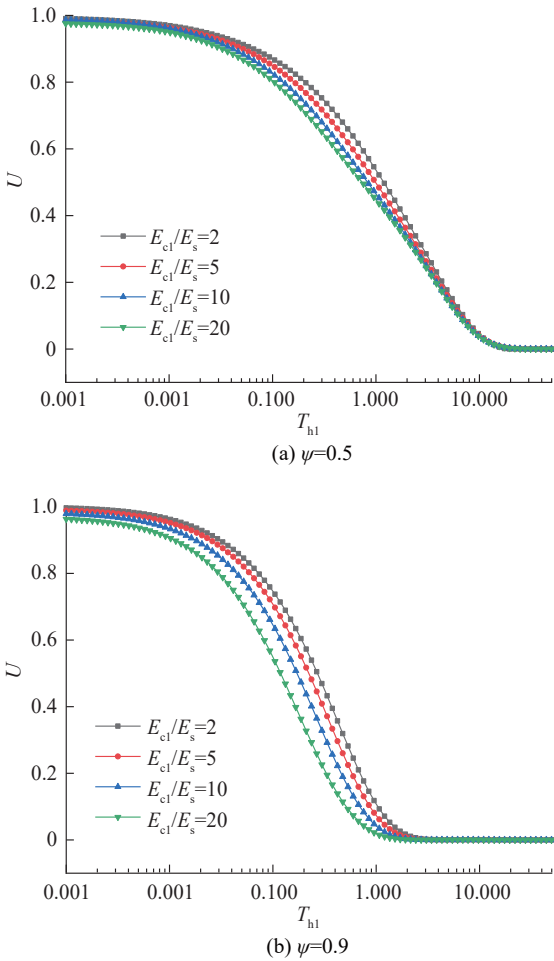


图 12 桩体压缩模量对复合地基固结度的影响

Fig. 12 Influence of compression modulus of stone columns on consolidation degree of composite foundation

4 结论

本文对长板-短桩多元排水体复合地基建建立计算模型,基于等应变假设与达西渗流定律,通过对碎石桩端以下复合地基建建立虚拟碎石桩,考虑土体径向固结与孔压、渗流连续性条件与涂抹效应,推导了长板-短桩多元排水体复合地基固结方程,并给出瞬时荷载与多级瞬时荷载下的固结度与孔压解答。最后,通过案例验证了解答的合理性,并对长板-短桩多元排水体复合地基固结性状进行分析,得到如下结论:

1)若按碎石桩与排水板等长条件下的多元排水体复合地基解析解来计算长板-短桩多元排水体复合地基工程的固结沉降问题,会高估复合地基固结度,尤其是复合地基后期的固结度,对工程安全极为不利,而本文解答可较好地工程实际提供依据。

2)随贯入度增大,碎石桩排水影响深度越大,更多的土中水可从碎石桩排出,长板-短桩多元排水体复合地基后期固结度有较大提升,但固结前期主要为上层土体孔隙水固结,因此,增大贯入度对固结前期速

率影响较小。

3)桩体周围涂抹系数变化对长板-短桩多元排水体复合地基固结影响较大, α_{c1} 越大,涂抹效应越强,复合地基固结速率越慢。而排水板涂抹系数 α_w 增大虽然也能影响复合地基固结速率,但由于其排水板规格限制,扰动区面积较小,因此对复合地基固结速率影响较弱。

4)长板-短桩多元排水体复合地基固结随排水板数量增多与渗透系数变大而逐渐加快,贯入度越低,排水板对固结后期的加速效果越强。

5)增大桩体渗透系数和压缩模量可显著加快长板-短桩多元排水体复合地基固结前中期的速率,且随贯入度增大,影响效果越显著。然而由于长板-短桩多元排水体复合地基固结后期主要为碎石桩端以下地基进行固结,因此,贯入度越低,增大桩体渗透系数和压缩模量对加速复合地基后期固结的影响越小。

参考文献:

- [1] Liu Songyu, Zhou Jian, Zhang Dingwen, et al. State of the art of the ground improvement technology in China[J]. China Civil Engineering Journal, 2020, 53(4): 93-110. [刘松玉, 周建, 章定文, 等. 地基处理技术进展[J]. 土木工程学报, 2020, 53(4): 93-110.]
- [2] Wang Shuang, Wang Rui, Yang Biao, et al. Simplified analysis for consolidation of stone columns reinforced foundation under general time-dependent loading[J]. Rock and Soil Mechanics, 2015, 36(1): 34-40. [王双, 王睿, 杨彪, 等. 变荷载作用下碎石桩复合地基固结简化分析[J]. 岩土力学, 2015, 36(1): 34-40.]
- [3] Tian Xiaojun. Study on settlement development of composite ground with adhesive columns[D]. Hangzhou: Zhejiang University, 2016. [田效军. 粘结材料桩复合地基固结沉降发展规律研究[D]. 杭州: 浙江大学, 2016.]
- [4] Lu Mengmeng, Bai Yao, Li Hongjun, et al. Analytical models and solutions for consolidation of composite foundation with multiple types of reinforcements[J]. Chinese Journal of Rock Mechanics and Engineering, 2021, 40(Supp2): 3301-3312. [卢萌盟, 白垚, 李红军, 等. 多元组合桩复合地基固结解析模型与解答[J]. 岩石力学与工程学报, 2021, 40(增刊2): 3301-3312.]
- [5] Jia Qingshan. Experimental study and engineering application of plastic drainage plate and gravel pile in comprehensive treatment of soft soil foundation of large oil tank [J]. Petroleum Processing and Petrochemicals, 1999, 30(8): 50-56. [贾庆山. 塑料排水板与碎石桩综合处理大型油罐软土地基的试验研究与工程应用[J]. 石油炼制与化工, 1999, 30(8): 50-56.]
- [6] Yang Ping, An Xin, Wang Jianxiu, et al. Drain consolidation

- settlement of hydraulic fill reinforced by gravel pile and dewatering plastic[C]//2011 AASRI Conference on Information Technology and Economic Development(AASRI-ITED 2011 V3),Kuala Lumpur: Intelligent Information Technology Application Association,2011:233-236.
- [7] Xu Jun,Han Wenxi,Wei Hao,et al.Numerical simulation of treatment effect of gravel pile combined with PVD preloaded soft foundation[J].Building Structure,2020,50(Supp2):679-684.[徐俊,韩文喜,魏浩,等.碎石桩联合PVD软基处理效果数值模拟[J].建筑结构,2020,50(增刊2):679-684.]
- [8] Xu Jun.Analysis and calculation of the post-construction settlement of the gravel pile+plastic drain board composite foundation of chengdu new airport[D].Chengdu:Chengdu University of Technology,2021.[徐俊.成都新机场碎石桩+排水板复合地基工后沉降预测研究[D].成都:成都理工大学,2021.]
- [9] Zhao Weibing,Ai Yingbo,Zhang Jing.Study on post-construction settlement of thick soft roadbed improved by drainage preloading[J].Hydro-Science and Engineering,2003,25(1):28-33.[赵维炳,艾英钵,张静.排水固结加固高速公路深厚软基工后沉降[J].水利水运工程学报,2003,25(1):28-33.]
- [10] Zhou Yadong,Zheng Qidan,Guo Shuaijie.Nonlinear consolidation model of composite foundation with partially penetrated stone column[J].Computers and Geotechnics,2023,161:105621.
- [11] Ye Guanbao,Chen Jian,Xing Haofeng,et al.In-situ tests on consolidation of composite foundation composed of short cement-soil piles and long plastic drainage plates[J].Journal of Tongji University(Natural Science),2010,38(12):1725-1729.[叶观宝,陈健,邢皓枫,等.长板-短桩组合型复合地基固结特性试验[J].同济大学学报(自然科学版),2010,38(12):1725-1729.]
- [12] Dong Bichang,Zhang Mingxuan,Zhang Pengfei,et al.Study on bearing capacity of dredger fill foundation treated by D-M method[J].Journal of Wuhan University of Technology(Transportation Science & Engineering),2021,45(2):303-307.[董必昌,张明轩,张鹏飞,等.长板-短桩工法处理吹填土地基承载性能研究[J].武汉理工大学学报(交通科学与工程版),2021,45(2):303-307.]
- [13] Lu Hua,Gao Quanchen,Zhou Bo,et al.Experimental research on bearing capacity of long-and-short pile composite foundation[J].Chinese Journal of Underground Space and Engineering,2015,11(1):56-63.[陆华,高全臣,周波,等.长短组合桩复合地基承载性状的试验研究[J].地下空间与工程学报,2015,11(1):56-63.]
- [14] Ye Guanbao,Liao Xingyue,Gao Yanbin,et al.Numerical analysis of improved deep soft foundation for highways by use of D-M method[J].Chinese Journal of Geotechnical Engineering,2008,30(2):232-236.[叶观宝,廖星樾,高彦斌,等.长板-短桩工法处理高速公路软土地基的数值分析[J].岩土工程学报,2008,30(2):232-236.]
- [15] Si Haiyan,Chang Hongtao,Chen Quanying,et al.Centrifugal model tests on D-M method[J].Chinese Journal of Geotechnical Engineering,2011,33(Supp1):406-409.[司海燕,裘红涛,陈全营,等.基于离心模型试验的长板-短桩工法研究[J].岩土工程学报,2011,33(增刊1):406-409.]
- [16] Xing Haofeng,Zhang Zhen,Ye Guanbao,et al.Simplified analysis for drainage system of composite foundation improved by cement-mixing columns and vertical drains[J].Journal of Tongji University(Natural Science),2011,39(5),656-660.[邢皓枫,张振,叶观宝,等.长板-短桩复合地基排水系统简化分析[J].同济大学学报(自然科学版),2011,39(5):656-660.]
- [17] Yu Chunliang,Zhang Aijun,Wang Yuguo,et al.Analytical solution for consolidation of combined composite foundation reinforced with penetrated impermeable columns and partially penetrated permeable stone columns[J].Computers and Geotechnics,2020,124:103606.
- [18] Lu Mengmeng,Zhang Qiang,Jing Hongwen,et al.Consolidation of band-shaped drain based on equivalent annular drain[J].Chinese Journal of Rock Mechanics and Engineering,2018,37(2):513-520.[卢萌萌,张强,靖洪文,等.基于环形等效的排水板地基固结[J].岩石力学与工程学报,2018,37(2):513-520.]
- [19] Huang Shenggen,Xiang Liliang,Yin Xin.Consolidation theory of PVD-DMM composite foundation based on equivalent annular drain[J].Journal of Railway Engineering Society,2021,38(11):15-21.[黄生根,向黎亮,殷鑫.基于环形等效的长板-短桩复合层固结理论[J].铁道工程学报,2021,38(11):15-21.]
- [20] Xie Kanghe,Zhou Kaimao.Consolidation theory for soft soil with partially penetrated vertical drains[J].Chinese Journal of Geotechnical Engineering,2006,28(6):679-684.[谢康和,周开茂.未打穿竖向排水井地基固结理论[J].岩土工程学报,2006,28(6):679-684.]
- [21] Fellenius B H,Castonguay N G.The efficiency of band shaped drains:A full scale laboratory study[R].National Research Council and the Industrial Research Assistance Programme,1985.
- [22] Lu Mengmeng,Sloan S W,Indraratna B,et al.A new analytical model for consolidation with multiple vertical drains[J].International Journal for Numerical and Analytical Methods in Geomechanics,2016,40(11):1623-1640.
- [23] Lu Xiangzong,Li Chuanxun.Consolidation solution for co-

- composite foundation with vertical drains-stone columns considering radial and vertical flow in soft soils[J]. *Engineering Mechanics*, 2025, 42(4): 187–196. [陆向综, 李传勋. 径竖向渗流下竖井-碎石桩复合地基固结解[J]. *工程力学*, 2025, 42(4): 187-196.]
- [24] Orleach P. Techniques to evaluate the field performance of vertical drains[D]. Cambridge: Massachusetts Institute of Technology, 1983.
- [25] Lu Mengmeng, Jing Hongwen, Zhou Yang, et al. General analytical model for consolidation of stone column-reinforced ground and combined composite ground[J]. *International Journal of Geomechanics*, 2017, 17(6): 04016131.
- [26] Tang Xiaowu, Niu Ben, Cheng Guanchu, et al. Closed-form solution for consolidation of three-layer soil with a vertical drain system[J]. *Geotextiles and Geomembranes*, 2013, 36: 81–91.
- [27] Zhou Kaimao. Study on the consolidation theory of soft soil with partially penetrated vertical drains[D]. Hangzhou: Zhejiang University, 2006. [周开茂. 未打穿砂井地基固结理论研究[D]. 杭州: 浙江大学, 2006.]
- [28] Ye Guanbao, Zhang Zhen, Han Jie, et al. Performance evaluation of an embankment on soft soil improved by deep mixed columns and prefabricated vertical drains[J]. *Journal of Performance of Constructed Facilities*, 2013, 27(5): 614–623.
- [29] Zhang Z, Ye G, Xing H. Consolidation analysis of soft soil improved with short deep mixed columns and long prefabricated vertical drains(PVDs)[J]. *Geosynthetics International*, 2015, 22(5): 366–379.
- [30] Li Chuanxun, Lu Xiangzong, Wu Wenbing, et al. An analytical solution for consolidation of soils with stone columns and vertical drains by considering the deformation of stone columns[J]. *Computers and Geotechnics*, 2023, 158: 105377.
- [31] Sun Jinxin, Lu Mengmeng, Han Bolin. Analytical solutions for consolidation of combined composite ground reinforced by short impervious columns and long PVDs[J]. *International Journal of Geomechanics*, 2023, 23(10): 04023169.

Analytical Models and Solutions for Consolidation of Composite Foundation with Long Prefabricated Vertical Drains and Short Stone Columns Based on Virtual Pile Method

XU Baolong, LU Mengmeng*, ZHANG Xinyan, LIU Yuanjie

(School of Mechanics and Civil Engineering, China University of Mining and Technology, Xuzhou 221116, China)

Abstract:

Objective The combined composite foundation with long prefabricated vertical drains (PVDs) and short stone columns demonstrates significant engineering benefits in practical applications by integrating reinforcements with varying drainage capacities. However, its consolidation characteristics remain insufficiently understood, resulting in a lack of strong theoretical support for engineering practices. In this context, the consolidation of the entire foundation is considered in two parts: consolidation within the length of the drainage piles and consolidation beneath the bottom of the drainage piles. Previous research has shown that the primary and secondary consolidation settlements of the soil layer beneath the bottom of the drainage piles are often the main contributors to excessive post-construction settlement. Therefore, particular attention is required for the consolidation theory of the combined composite foundation with multiple drains under this condition.

Methods Taking the four common layout forms of composite foundations with stone columns-PVDs in engineering into account, the consolidation analytical model for the composite foundation with long PVDs and short stone columns was established, which considered stone columns as the central element and PVDs as the outer boundary. The PVDs of the outer boundary were reasonably simplified into an outer drainage ring using the area equivalent method. The composite foundation with long PVDs and short stone columns was divided into two layers: the upper layer, which was the composite foundation within the length of the stone columns, and the lower layer, which extended from below the bottom of the stone columns to the depth of the composite foundation. A virtual pile was assumed to exist at the bottom of the stone columns, with consolidation parameters identical to the surrounding soil, to ensure continuity conditions of pore pressure and seepage between the upper and lower layers of the foundation. Based on the assumption of equal strain, the smear effect during the installation of multiple drains and the radial bidirectional seepage toward the stone columns and PVDs within the soil were fully considered. The consolidation control equations were derived separately for the upper and lower layers of the composite foundation by incorporating these factors. During the consolidation process, it was assumed that the surface of the foundation was drained, and the bottom was not drained. The classical assumption of equal flow around the drains was applied to the boundary between the stone columns and the soil, as well as the boundary between the PVDs. Utilizing the method of separated variables, linear equations, properties of singular matrices, and the trigonometric orthogonality of pore pressure in the composite foundation, the analytical solutions for pore pressure and average consolidation degree of the composite foundation, soil, stone columns, and PVDs under instantaneous loads were derived for the upper, lower, and overall layers of the composite foundation. In addition, employing the superposition method, the solu-

tion of consolidation under k -level multi-stage instantaneous loading conditions was obtained. Finally, the analytical solution result of the composite foundation with long PVDs and short stone columns was compared to the settlement data of an embankment project in Shanghai. The analytical solution demonstrated strong agreement with the measured settlement data of the project, indicating that the analytical solution of consolidation for the composite foundation with long PVDs and short stone columns accurately predicted settlement with high rationality and reliability.

Results and Discussions A parametric sensitivity analysis was conducted to investigate consolidation behavior and optimize the methods of this composite foundation. The results showed that quantifying the acceleration effect of the composite foundation with long PVDs and short stone columns compared to traditional composite foundations with long PVDs and short soil-cement piles, the former significantly accelerated the consolidation rate, with a maximum difference of 15.9%. Increasing the penetration ratio effectively enhanced the consolidation rate of the composite foundation, with a more significant impact on the later stages of consolidation. In addition, augmenting the permeability coefficient and compression modulus of stone columns accelerated the early stages of foundation consolidation, and this influence became increasingly pronounced as the penetration ratio increased. Unlike the impact of stone column parameters on consolidation, increasing the number and permeability coefficient of PVDs also accelerated the rate of foundation consolidation, with a stronger effect in the later stages. The smear effect of stone columns has a significant influence on the composite foundation, whereas the smear effect of PVDs exerts a relatively weaker impact on the consolidation rate of the composite foundation due to their smaller size.

Conclusions The results indicate that the analytical solutions correspond closely with the measured settlement data, establishing a reliable basis for practical engineering applications of the composite foundation under study. In addition, in comparison to traditional composite foundations consisting of long PVDs and short soil-cement piles, the configuration with long PVDs and short stone columns demonstrates clear advantages in the consolidation rate. Therefore, this research provides both significant theoretical insights and practical contributions. The parametric sensitivity analysis reveals that the effects of long stone column parameters and short PVD parameters on the consolidation rate differ considerably. The consolidated solutions and characteristic analyses of the composite foundation with long PVDs and short stone columns can not only provide guidance for related engineering foundations but also act as a reference for optimizing the application of this technology to attain greater engineering benefits.

Key words: consolidation; analytical solution; composite foundation; stone column; prefabricated vertical drain (PVD)

(编辑 周璇)

引用格式: Xu Baolong, Lu Mengmeng, Zhang Xinyan, et al. Analytical models and solutions for consolidation of composite foundation with long prefabricated vertical drains and short stone columns based on virtual pile method[J]. *Advanced Engineering Sciences*, 2025, 57(6): 242-255. [许宝龙, 卢萌盟, 张鑫岩, 等. 基于虚拟桩法的长板-短桩多元排水体复合地基固结模型与解答[J]. *工程科学与技术*, 2025, 57(6): 242-255.]